



The interplay between subduction and lateral extrusion: A case study for the European Eastern Alps based on analogue models



I.E. van Gelder^{a,*}, E. Willingshofer^a, D. Sokoutis^{a,b}, S.A.P.L. Cloetingh^a

^a Utrecht University, Faculty of Geosciences, Utrecht, The Netherlands

^b University of Oslo, Department of Geosciences, Oslo, Norway

ARTICLE INFO

Article history:

Received 1 December 2016

Received in revised form 21 April 2017

Accepted 10 May 2017

Available online 30 May 2017

Editor: A. Yin

Keywords:

subduction

lateral extrusion

analogue modelling

Eastern Alps

ABSTRACT

A series of analogue experiments simulating intra-continental subduction contemporaneous with lateral extrusion of the upper plate are performed to study the interference between these two processes at crustal levels and in the lithospheric mantle. The models demonstrate that intra-continental subduction and coeval lateral extrusion of the upper plate are compatible processes leading to similar deformation structures within the extruding region as compared to the classical setup, lithosphere-scale indentation. Strong coupling across the subduction boundary allows for the transfer of stresses to the upper plate, where strain regimes are characterized by crustal thickening near a confined margin and dominated by lateral displacement of material near a weak lateral confinement. The strain regimes propagate laterally during ongoing convergence creating an area of overlap characterized by transpression. When subduction is oblique to the convergence direction, the upper plate is less deformed and as a consequence the amount of lateral extrusion decreases. In addition, strain is partitioned along the oblique plate boundary resulting in less subduction in expense of right lateral displacement close to the weak lateral confinement. Both oblique and orthogonal subduction models have a strong resemblance to lateral extrusion tectonics of the Eastern Alps (Europe), where subduction of the adjacent Adriatic plate beneath the Eastern Alps is debated. Our results imply that subduction of Adria is a valid mechanism to induce extrusion-type deformation within the Eastern Alps lithosphere. Furthermore, our findings suggest that the Oligocene to Late Miocene structural evolution of the Eastern Alps reflects a phase of oblique subduction followed by a later stage of orthogonal subduction conform a Miocene shift in the plate motion of Adria. Oblique subduction also provides a viable mechanism to explain the rapid decrease in slab length of the Adriatic plate beneath the Eastern Alps towards the Pannonian Basin.

© 2017 Elsevier B.V. All rights reserved.

1. Introduction

Lateral extrusion entails the combined effects of tectonic escape and gravitational collapse of a weak orogenic wedge in response to indentation under conditions of an unconstrained (mechanically weak) lateral boundary (Ratschbacher et al., 1991a). This process results in the escape of crustal blocks along conjugate strike-slip faults towards a weak boundary (i.e. a coevally extending region) oriented at a high angle to the convergence direction. The Eastern Alps (Europe), Tibetan Plateau, and the Anatolian Plateau, for instance (Fig. 1a), have been subjected to this process with variable contributions of the collapse component (e.g., McKenzie, 1972; Ratschbacher et al., 1991a; Tapponnier et al., 1986).

* Correspondence to: Utrecht University, Department of Earth Sciences, PO Box 80021, 3508 TA Utrecht, The Netherlands.

E-mail address: inge_van_gelder@hotmail.com (I.E. van Gelder).

Previous numerical and analogue modelling studies yielded valuable insights in the parameter space favoring escape and extrusion tectonics. These studies have shown that a weak lateral boundary is a pre-requisite for lateral extrusion to occur (Davy and Cobbold, 1988; Faccenna et al., 1996) and that the indenter only needs to be moderately strong in comparison to the indented region (Robl and Stüwe, 2005; Willingshofer et al., 2005). Other important parameters influencing the extrusion process and the resulting deformation geometries are the shape of the indenter, the convergence direction or the width and rheological variations of the indented region (e.g., Ratschbacher et al., 1991b; Rosenberg et al., 2007; Sokoutis et al., 2000).

The Eastern Alps in Europe (Fig. 1b) is one of the key examples for the study of lateral extrusion tectonics (e.g., Frisch et al., 2000; Ratschbacher et al., 1991a; Wölfler et al., 2011). There, extrusion is driven by Miocene northward indentation of the Eastern Alps lithosphere by the Adriatic microplate, which occurred simultaneously with the opening of the Pannonian Basin in the east (e.g.,

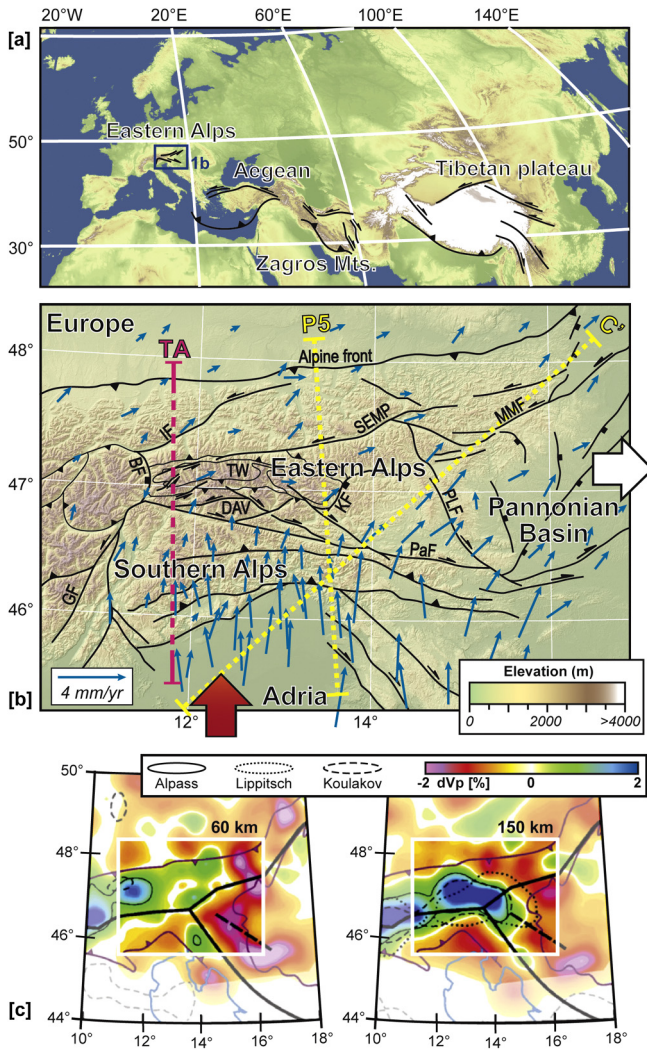


Fig. 1. [a] Topographic map showing the various regions that are affected by lateral extrusion coeval with subduction or indentation. The blue box outlines the area shown in Fig. 1b. [b] The elevation map of the Eastern Alps overlain by the major faults and structures associated with lateral extrusion in the Eastern Alps (modified after: Ratschbacher et al., 1991a; Schmid et al., 2004). The white arrow indicates the average direction of Pannonian back-arc extension and the red arrow indicates the direction of indentation or subduction of the Adriatic plate. The yellow dashed lines show the location of the tomographic sections presented in Fig. 7c and the pink line show the location of the TranALP (TA) seismic section (Figs. 7a and b). The scaled blue arrows represent the present day GPS displacements extracted from Metois et al. (2015). [c] Two tomographic slices at 60 and 150 km depth by Mitterbauer et al. (2011). The highlighted area coincides with the map in Fig. 1b and the slices also show the tomographic interpretations of the area according to Lippitsch et al. (2003); Koulakov et al. (2009); Mitterbauer et al. (2011). Abbreviations: Mur–Mürz fault (MMF), Peradriatic fault (PaF), Guidicarie fault (GF), Deferegg–Antholz–Vals fault (DAV), Pöls–Lavanttal fault (PLF), Salzach–Ennstal–Mariatzell–Puchberg fault (SEMP), Brenner fault (BF), Katschberg fault (KF), Innthal fault (IF), Vienna Basin (VB).

Ratschbacher et al., 1991a). The latter is related to the Carpathian slab roll-back and created the space needed for the extruding crustal blocks. Within this tectonic frame the Adriatic plate is traditionally considered as a semi-rigid indenter (Ratschbacher et al., 1991a) and marks the southern border of the weak Eastern Alps lithosphere, which is bounded to the north by the strong European lithosphere (Fig. 1b). Controversially, high-resolution teleseismic tomography as interpreted by Lippitsch et al. (2003) suggests that the Adriatic plate is not a lithosphere-scale bulldozer pushing against the Alps but has been subducting beneath the extruding Eastern Alps since about 30 Ma (Handy et al., 2015). Although interpretations of tomographic data differ (see discussion

in Mitterbauer et al., 2011) (Fig. 1c), these findings raise first order questions such as: (a) how deformation is partitioned between the laterally extruding upper plate and the subducting lower plate, (b) what is the role of upper and lower plate rheology and geometry, and (c) what mechanisms control the upper plate deformation. These questions are not only relevant for the Eastern Alps but also the Tibetan Plateau, the Anatolian Plateau or the Zagros Mountains (Fig. 1a), where lateral extrusion occurs in the upper plate of a subducting continental plate.

We present results of a physical analogue modeling study that for the first time embarks on the interplay between intra-plate subduction and lateral extrusion processes, assessing the sensitivity of upper plate extrusion-type deformation in response to orthogonal and oblique continental subduction. The modelling results are primarily compared to the structural evolution of the Eastern Alps, where the extracted interferences contribute to the debate of indentation versus subduction of the Adriatic plate.

2. Experimental approach

We present lithosphere-scale physical analogue modelling results in which we compare the results of a classical indentation-extrusion scenario with that of a combined subduction-extrusion setting with the plate geometry as an additional variable. The experiments have been designed to allow for a first-order comparison with the Eastern Alps, but are from a conceptual point of view also applicable to other regions affected by lateral extrusion coeval to indentation or subduction, such as Tibet or the Aegean.

2.1. Experimental set-up and rheology

The setup of the experiments (Fig. 2) incorporates continental collision perpendicular to a weak lateral confinement, where continental collision is either activated by: a) indentation (experiment 1), or b) subduction (experiments 2 and 3). The weak lateral confinement mimics the opening of the Pannonian Basin and facilitates flow of the lower crust and upper mantle of the indented region perpendicular to the convergence direction.

For the weak lateral confinement we used a low viscosity and low density silicon putty (Table 1), which is placed along the entire length of the model. Initially the weak confinement is fixed during model build-up by a 5 cm broad wooden block to prevent flow of the material. At the start of the model run the fixation is removed creating an open space that allows for the weak confinement to flow (spread) freely onto the experimental asthenosphere, thereby provoking orogen parallel extension of the upper plate (see also movies 1–3). The orogen parallel elongation coupled to coeval indentation or subduction ultimately leads to laterally extruding lithospheric material, perpendicular to the direction of shortening.

In all experiments the modeled continental lithospheres consist of a brittle upper crust, a ductile lower crust and a ductile upper mantle. Strength calculations of Willingshofer and Cloetingh (2003) suggest that the Eastern Alps lithosphere is weak in comparison to the subducting or indenting Adriatic lithosphere. This strength contrast along with the approximate crustal thicknesses obtained from the TRANSALP seismic profile (TRANSALP Working Group, 2002, see also Fig. 7b) are used to constrain the initial model setup. Note that instead of using a rigid indenter (Ratschbacher et al., 1991b; Rosenberg et al., 2007) we deploy a system where the indenter and the subducting plates have a pre-defined rheological stratification (Fig. 2) and are pushed against the deformable region through the advancement of an automated moving wall. In all experiments the rate and amount of convergence was the same, namely 1 cm/h with a total of 8 cm of shortening. The velocity

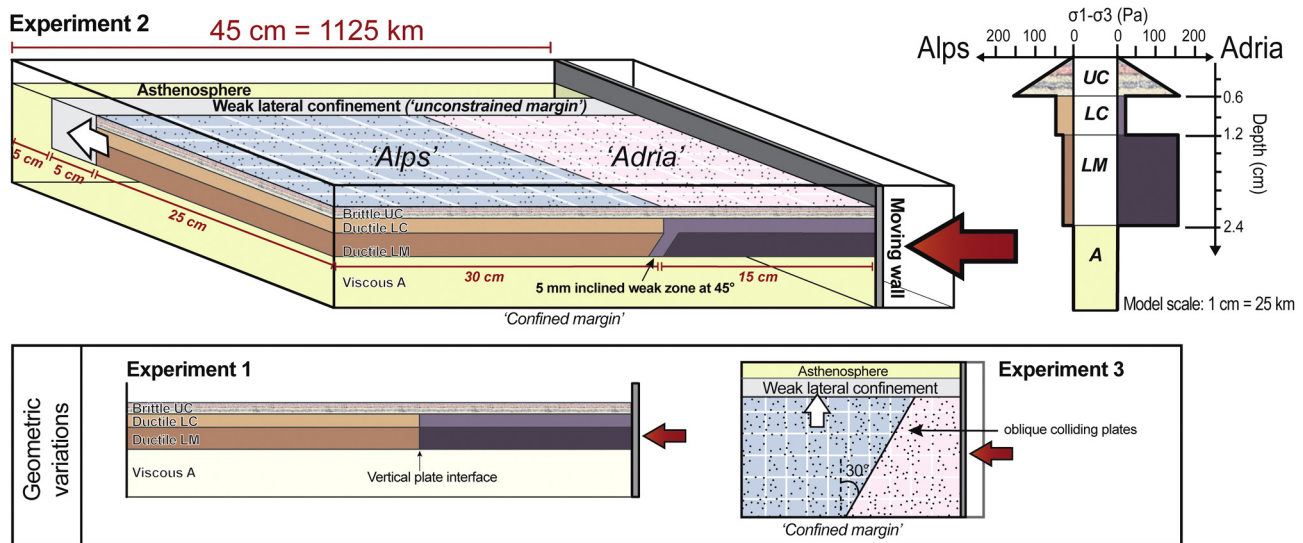


Fig. 2. The experimental set-up showing the different parameters incorporated into the model. The figure also presents the strength profiles for the upper and lower plate. Abbreviations: upper crust (UC), lower crust (LC), lithospheric mantle (LM), asthenosphere (A).

scales to 1.25 cm/a in nature, slightly higher than an average convergence velocity of 0.7 cm/a when assuming that at least 200 km of shortening took place during the last 30 Ma in the Eastern Alps (Ustaszewski et al., 2008).

In the experiment with indentation the model has a vertical plate contact, whereas an inclined weak boundary at the level of the lithospheric mantle is implemented to initiate intra-plate subduction (experiments 2 and 3), simulating the effect of pre-existing structures following the procedure of Luth et al. (2010). The onset of subduction of the Adriatic plate is proposed to be the result of large scale crust-mantle decoupling of both the Alpine and Adriatic lithosphere (Handy et al., 2015). Nevertheless, the rheological make-up enables the transfer of stress in order to obtain upper plate deformation (Iaffaldano et al., 2012; Sokoutis and Willingshofer, 2011). Therefore, the experiments incorporated a lower crust in both the upper and lower plate, which can behave as a decoupling horizon (Fig. 2), whereas the strength contrast between the plate interface and the lithospheric mantle of the upper plate allows for the transfer of stress.

2.2. Material properties and scaling

The brittle crust in the experiments is simulated by dry feldspar sand showing a Mohr–Coulomb-type behavior while the ductile layers are composed of silicon putty (PDMS polymer and/or rhodorsil gomme, see Table 1) with quasi-Newtonian behavior. To obtain the desired density the silicon putty is mixed with quartz sand and barium-sulfate as fillers and oleic acid to adjust the viscosity. The model lithosphere overlies a high density and low viscosity fluid mixture representing the asthenosphere, which allows for isostatic compensation (Fig. 2). The exact dimensions and material properties of all the individual layers are summarized in Table 1 and presented in Fig. 2 together with strength profiles for the modeled lower and upper plate.

The used materials and dimensions are scaled to achieve geometrical, dynamic and rheological similarity between nature and model, following detailed descriptions in Weijermars and Schmelting (1986) and Davy and Cobbold (1991). For this purpose the Ramberg number (Rm, the ratio between gravitational and viscous stresses) has been calculated for ductile layers and the Smoluchowsky number (Sm, the ratio between gravitational stress and cohesive strength) for the brittle layers (Table 1). Both equations and explanations are presented in Ramberg (1981) and in

Sokoutis et al. (2005), the latter directly applied to analogue modelling.

The overall stress-scale factor for the experiments is expressed by:

$$\sigma^* = \rho^* g^* h^* \quad (1)$$

where σ , ρ , g and h refer to stress, density, gravitational acceleration (9.81 m/s^2) and thickness of the layers and the asterisk refers to the model versus nature ratio. Based on the model material properties (Table 1) and their equivalent properties in nature (see also Luth et al. (2010)), we obtain a stress ratio of approximately 2.5×10^{-7} implying a geometrical scale of 1 cm in the model equals 25 km in nature. Hence, the applied 8 cm of shortening equals to 200 km in nature, this is in line with the estimated 200 km of Alps–Adria convergence during the last 30 Ma (Ustaszewski et al., 2008) and the estimated 210 km of subduction of Adria beneath the Eastern Alps (Fig. 7b; Lippitsch et al., 2003).

2.3. Explored parameter space

The main target of the experimental series is to demonstrate the effect of subduction on lateral extrusion (experiment 2) as opposed to the classical tectonic setting where lateral extrusion occurs contemporaneous with indentation (experiment 1). Additionally, we studied the influence of oblique convergence (experiment 3) on the distribution of strain in the upper plate. The straight plate geometry used in experiment 1 and 2 is similar to the current Adria–Eastern Alps contact, whilst the oblique geometry represents the setting prior to a possible 20° counterclockwise rotation of Adria as indicated by paleomagnetic data (Márton et al., 2003) or prior to changes in convergence direction, i.e. from a NNE-directed to NW-directed motion of Adria (Caputo et al., 2010).

2.4. Experiment recordings

During the experimental runs the model surface is monitored by automated top-view photographs at regular time intervals. These photos are subsequently utilized to visualize the incremental deformation through time using the Particle Image Velocimetry (PIV) analysis technique (Westerweel, 1997). For this method we used the open source software MatPIV (Sveen, 2004) for Matlab®

Table 1
The material and scaling properties used in the experimental set-up.

	Material	Density ρ (kg m ⁻³)	Thickness layer (m)	Friction coefficient μ	Cohesion C (Pa)	Stress component n	Material constant A	Strain rate (s ⁻¹)	Effective viscosity η (Pa·s)	S_m	R_m
<i>Alps</i>	Brittle crust	1300	6.0×10^{-3}	0.4–0.7	15–35	1.36	3×10^{-5}	4.6×10^{-4}	3.04×10^4	1.68	1.49
	<i>nature</i>	2750	2.4×10^4								
	Ductile crust	1420	6.0×10^{-3}								
	<i>nature</i>	2900	1.5×10^4								
Upper mantle	model	1530	1.5×10^{-2}	0.4–0.7	15–35	1.31	1×10^{-5}	1.9×10^{-4}	1.06×10^4	2.50	4.04
	<i>nature</i>	3300	7.0×10^4								
	<i>nature</i>										
<i>Adria and European foreland</i>	Brittle crust	1300	6.0×10^{-3}	0.4–0.7	15–35	1.3	2×10^{-5}	4.6×10^{-4}	2.28×10^4	1.68	1.98
	<i>nature</i>	2750	2.4×10^4								
	Ductile crust	1430	6.0×10^{-3}								
	<i>nature</i>	2900	1.5×10^4								
Upper mantle	model	1500	1.5×10^{-2}	0.4–0.7	15–35	2.7	6×10^{-6}	1.9×10^{-4}	2.00×10^5	2.06	31.09
	<i>nature</i>	3300	7.0×10^4								
Other	Lateral confinement	1360	2.1×10^{-2}	0.4–0.7	15–35	1.04	5×10^{-5}	1.3×10^{-4}	1.56×10^4	1.2	33.94
	<i>nature</i>	2900	4.0×10^4								
	Asthenosphere	1505									

^a a = Rhodorsil gomme CSIR (Rhône Poulenc, France), and b = polydimethylsiloxane polymer (PDMS).

providing surface vector fields for each specified time step. Detailed description of the PIV technique applied to analogue models is described in [Leever et al. \(2011\)](#).

To visualize the lithospheric scale response to lateral extrusion a grid of 5×5 cm was drawn on the bottom of the lithospheric mantle. Analyzing the distortions of this grid at the end of the experiment shows the accumulated strain in the lithospheric mantle. Structural analysis of the top and bottom layers has been complemented by sectioning after having wetted and frozen the experiments, providing valuable information on the internal deformation structures.

2.5. Experimental simplifications

The physical analogue models do not include surface processes nor take temperature and thus depth dependent changes of viscosity into account. We approach viscosity variations by implementing different viscosities for the lower crust and lithospheric mantle. This first-order approximation has been validated by [Davy and Cobbold \(1991\)](#). We consider surface processes to be of secondary importance, as the topographic build-up during lateral extrusion is low compared to head on collision. Furthermore, the models also include simplifications of geometric structures, by excluding pre-existing crustal thickness variations or inherited structures.

The implemented simplifications allow for an in-depth analysis of the feedback relations between the explored experimental parameters but should not be ignored when comparing the models to nature. Hence, we restrict our comparison with the Eastern Alps to the first-order features.

3. Results

Top view images through time, PIV surface analysis, mantle flow visualization and cross-sections of all individual experiments are presented in [Figs. 3, 4 and 5](#). Un-interpreted sections are available upon request. To enhance visualization and understanding of the experiments this paper features a video for each model showing the experimental run (see Supplementary online Movies 1–3).

3.1. Experiment 1: indentation

Experiment 1 ([Fig. 3](#)) displays the effect of indentation of a weak lithosphere contemporaneous with flow of the weak lateral confinement perpendicular to the convergence direction, which exerts spreading of the upper plate. The first structures observed ([Fig. 3c](#)) at 5% bulk shortening, are thrusts near the confined margin (i.e. the margin opposite to the unconstrained margin, see also [Fig. 2](#)) that are (sub-)parallel to the boundary of the indenter. Towards the weak lateral confinement the initial structures strike at a high angle to the convergence direction accommodating strike-slip displacements and spreading of the upper crust. The analysis of particle displacements reveal that the sinistral and dextral strike-slip faults bound a wedge-shaped domain with constant vector velocity ([Fig. 3c](#)). At 11% bulk shortening the strike-slip faults, both dextral and sinistral, are more clearly visible at the surface and thrusts are more pronounced forming pop-up structures. Both deformation styles form separate strain domains, i.e. they develop independently of each other. However, at 17% and 22% bulk shortening the areas dominated by strike-slip and shortening overlap which creates a complex pattern of cross-cutting faults and transpressive structures. The overlap is the result of lateral propagation of the initial domains that are either dominated by strike-slip or shortening kinematics. Notably, the indenter does not accommodate significant deformation in experiment 1, besides a dextral strike-slip fault near the lateral confinement and a dextral fault cross-cutting the plate contact.

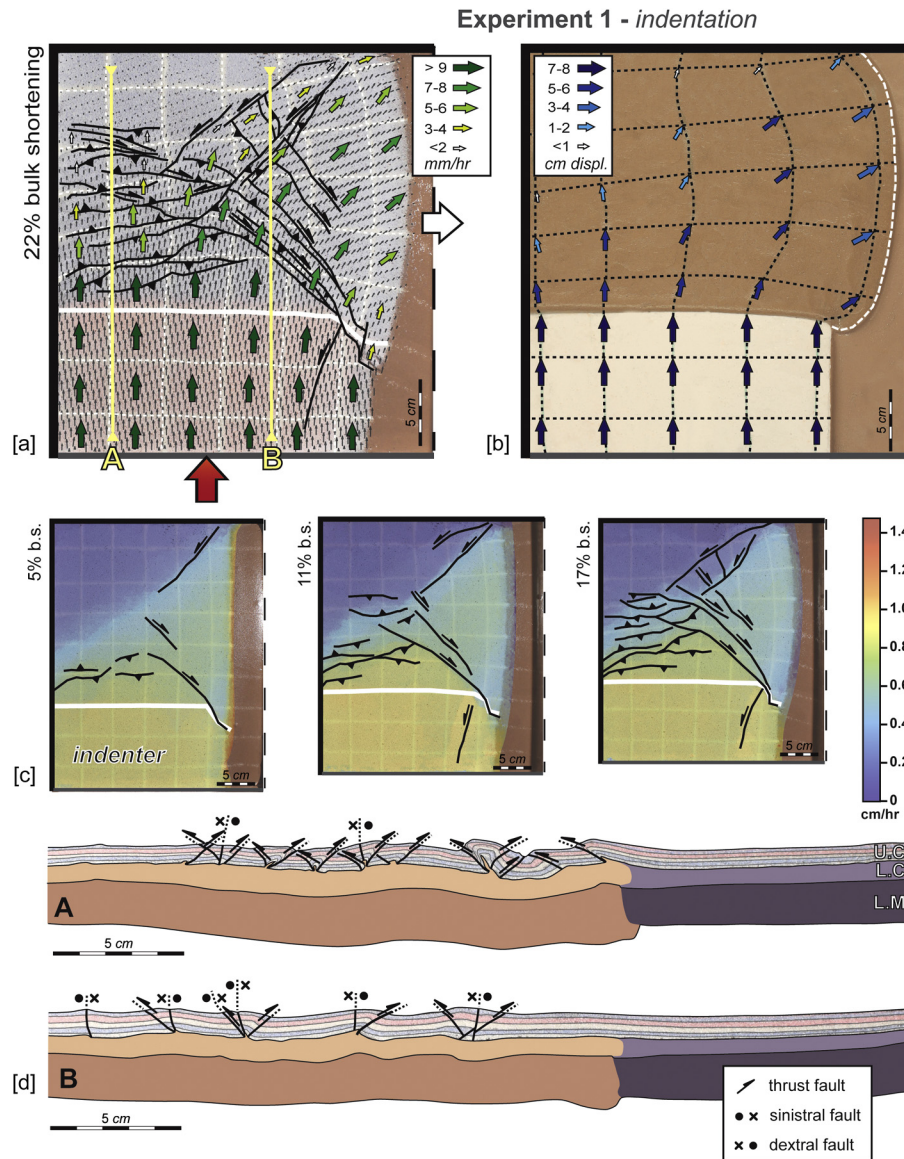


Fig. 3. Modeling results for experiment 1; **[a]** top-view image at the final stage of modelling (22% bulk shortening) overlain by the interpretation of crustal structures and the PIV velocity field from which we derived the simplified surface displacement for illustration purposes. The surface grid is 4 × 4 cm and the solid white line indicates the boundary between the two converging continental plates. **[b]** Bottom-view of the lithospheric mantle displaying the deformed grid and the displacement vectors. The dashed white line indicates the transition from the mantle layer to the weak lateral confinement. **[c]** Top view images through time, for 5, 11 and 17% bulk shortening overlain by the displacement velocity images (see scale bar to the right) and the interpretation of visible faults. The solid white line indicates the boundary between the two converging continental plates. **[d]** Cross-sections of the experiment. The yellow lines in Fig. 3a indicate where the cross-sections are located. Abbreviations: upper crust (UC), lower crust (LC), lithospheric mantle (LM), bulk shortening (b.s.).

The along strike variations in structural style (thrusting, transpression and strike-slip) are clearly visible in the cross-sections; cross-sections A of experiment 1 is dominated by thrust faulting and cross-sections B by strike-slip faulting (Fig. 3d). The cross-sections also confirm that the indenter is undeformed, i.e. no thickening or distortions are visible. Lithospheric thickening within the indented plate is mainly restricted to the upper crust, whilst the lower crust and lithospheric mantle do not appear to be affected by significant thickening. The minimal amount of thickening of the lithospheric mantle is in line with observed flow at the bottom of the lithospheric mantle (Fig. 3b), indicating that shortening has dominantly been accommodated by flow at high angle to the convergence direction. Quantitative analysis of lithospheric mantle versus surface deformation shows that the mantle layer has been elongated by 18% versus 14% elongation for the upper crust (Table 2). Furthermore, the cross-sections also indicate that the upper plate deformations that are observed in the brittle crust also affect

the lower crust such that the upper-lower crust boundary is offset where pop-up structures are present. These are also sites where upper mantle distortions occur, creating a pattern of lithospheric scale folding (section A, Fig. 3d). These observations suggest that the upper plate behaves as a coupled lithosphere.

The surface and lithospheric mantle displacements of the indenter (Figs. 3a and 3b) are identical, both characterized by vectors parallel to the convergence direction, with constant displacement velocity for the entire indenter through time (Fig. 3c). For the indented region the surface displacements near the confined margin are parallel to the shortening direction with decreasing velocities further away from the indenter. The thrusts and pop-up structures near the indenter accommodate a large portion of the convergence indicated by the strong decrease in displacement velocity across these structures (Fig. 3c). In front of the indenter the displacement vectors (Fig. 3a) have an increasing component of lateral displacement in the direction of the weak lateral component, i.e. vectors

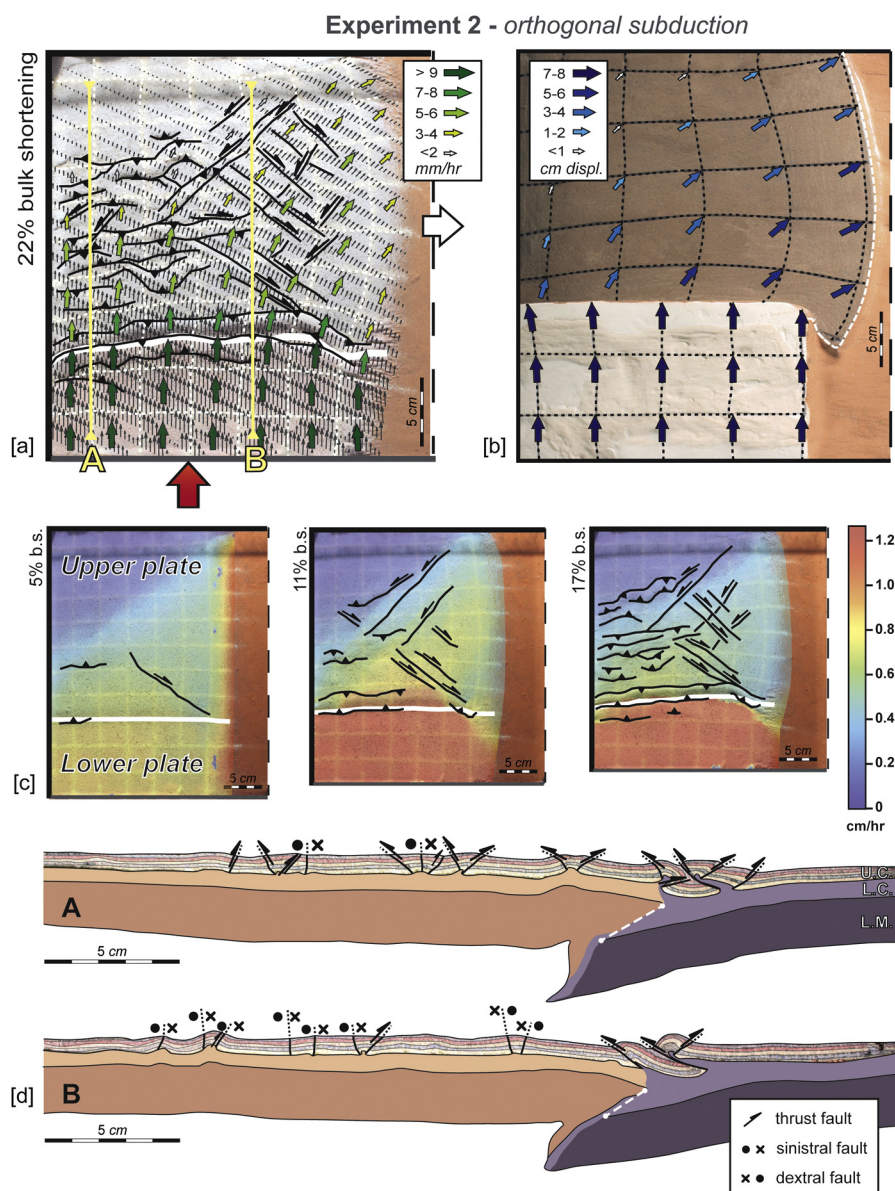


Fig. 4. Modeling results for experiment 2, see detailed figure description below Fig. 3.

strongly deviate from the convergence direction and rotate towards the weak lateral confinement. The displacement vectors at the surface and the lithospheric mantle have the highest displacement velocity at the center of the extruding wedge; at the surface this is a constant feature through time (Fig. 3c).

3.2. Experiment 2: orthogonal subduction

Experiment 2 (Fig. 4) explores lateral extrusion of the upper plate in response to subduction. During the initial stage of the experiment, shortening is accommodated within the upper plate by developing a wedge shaped domain indicated by the particle velocity image at 5% bulk shortening (Fig. 4c), which is similar to experiment 1. This wedge is bounded by a dextral and a sinistral strike-slip fault whereby the former developed earlier (at 5% bulk shortening) than the latter that emerges at 11% bulk shortening. At the same time a fore-thrust forms parallel to and at the position of the plate boundary which initiates near the confined margin and propagates with ongoing convergence towards the weak lateral confinement. At 11% bulk shortening the fore-thrust is accompanied by a back-thrust, transporting material onto

the upper plate where additional dextral faults and thrusts appear, the latter striking parallel to the plate boundary. From 11% up to 22% bulk shortening the deformation in the upper plate intensifies in a similar manner as in experiment 1, including the formation of cross-cutting faults and transpressional structures from 17% bulk shortening. In the meantime, surface deformation of the subducting plate migrates away from the plate boundary where a second pop-up structure develops. The back-thrust of the initial pop-up remains active, but the associated fore-thrust is over-thrust by the second pop-up. Both pop-ups are eminent along the confined margin but towards the unconstrained margin the strain is only accommodated by back-thrusts with a minor fore-thrust. Overall, the upper plate deformation is very similar to the indented region in experiment 1, but the deformation of the subducting plate distinguishes this experiment from the first one.

Lateral variations in structural style in the upper plate (i.e. shortening versus strike-slip dominated domains) are visible when comparing cross-sections A and B (Fig. 4d). The cross-sections also illustrate the subduction geometry of the lower plate, which is characterized by thrust and pop-up structures in the upper crust and bending of the upper mantle. Furthermore, the lower crust

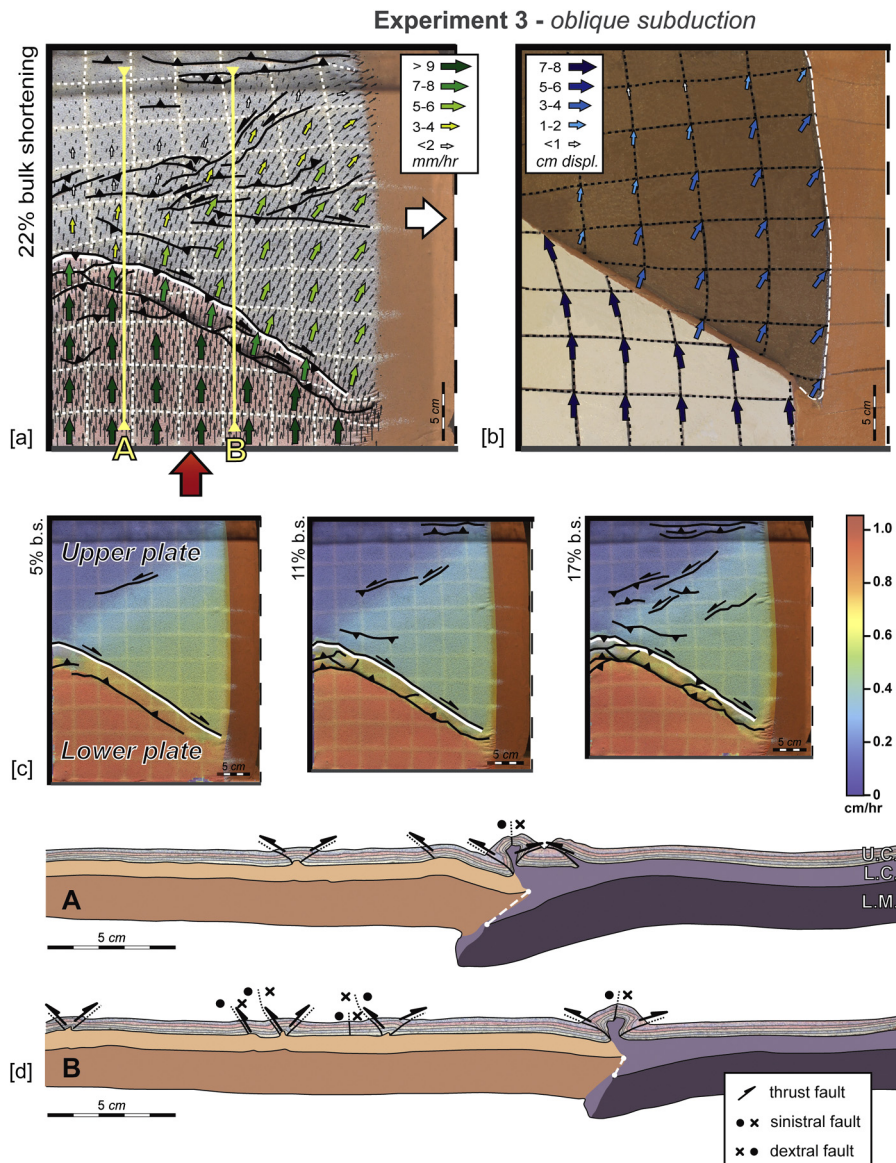


Fig. 5. Modeling results for experiment 3, see detailed figure description below Fig. 3.

in the lower plate partially follows the upper crust deformation but also partially subducts and is affected by thickening at the plate boundary, suggesting that the lower crust acts as a decoupling horizon allowing the upper mantle to subduct and to obtain foreland propagating thrusts in the upper crust. In the upper plate, both the lithospheric mantle and the lower crust are not thickened, yet a small part of the lithospheric mantle is being dragged down with the subducting boundary. Towards the weak lateral confinement cross-section B records less subduction by 15% compared to cross-section A (Table 2). This lateral variation is in line with an observed decrease in the amount of shortening accommodated along the plate boundary in the direction of the weak lateral confinement (see also Fig. 4a).

The vector field shows that the displacement patterns at the surface at 22% bulk shortening (Fig. 4a) is similar to the displacements recorded in the mantle layer (Fig. 4b) although the lateral component of displacement is greater in the mantle. These observations are alike the displacements recorded in experiment 1 (Figs. 3a and 3b). Contrasting to experiment 1 are the displacement velocities in the upper plate compared to the indented region. At the surface a strong decrease in the vector velocity is observed

when passing from the lower to the upper plate; this implies that the pop-up structures and the associated subduction accommodate a high amount of convergence. Furthermore, in this experiment the elongation factor (Table 2) for the lithospheric mantle (18%) is higher compared to the crust (12%).

3.3. Experiment 3: oblique subduction

Experiment 3 (Fig. 5) includes oblique subduction with respect to the convergence direction, which is implemented by the initial plate geometry (Fig. 2). Deformation occurs parallel to the oblique plate boundary, where at 5% bulk shortening, a fore- and back-thrust occurs (Fig. 5c). The back-thrust also accommodates dextral displacement, inferred from the grid distortions. The oblique back-thrust together with a minor sinistral fault in the upper plate bounds a wedge shaped domain supported by the displacement velocity image (Fig. 5c), suggesting that a broad domain of the upper plate is extruded. At 11% bulk shortening the previously mentioned structures continue to accommodate shortening and extrusion, but at 17% bulk shortening additional sinistral faults appear in the upper plate, as well as pop-up structures which develop at far distance from the plate boundary. The back-thrust along the

Table 2

The amount of extension, shortening and subduction for the three experiments and for the Eastern Alps (according to Frisch, 1998). The amount of subduction (slab length) is converted to km's according to the model scale (1 cm = 25 km). The amount of extension and shortening is calculated in percentages according to: $((\Delta L)/L_0) * 100\%$. Where ΔL is the measured length difference and L_0 is the initial length.

	Units	Models			Nature
		Exp. 1	Exp. 2	Exp. 3	
<i>Elongation</i>					
<i>Upper crust width at 0% and 25% bulk shortening</i>					
Width _{t=0}	cm	25	25	25	–
Width _{Δt}	cm	28.5	28	27.2	–
Elongation	%	14%	12%	9%	50%
<i>Upper mantle change in width at 0% and 25% bulk shortening</i>					
Width _{t=0}	cm	25	25	25	–
Width _{Δt}	cm	29.5	29.5	28	–
Elongation	%	18%	18%	12%	unknown
<i>Shortening upper crust</i>					
<i>Change in length along confined margin (West) from 0% to 25% bulk shortening</i>					
Length _{t=0}	cm	30	30	20	–
Length _{Δt}	cm	23	25.3	17.5	–
Shortening	%	23%	16%	13%	54%
<i>Change in length along unconstrained margin (East) from 0% to 25% bulk shortening</i>					
Length _{t=0}	cm	30	30	36	–
Length _{Δt}	cm	24.5	25.7	31.7	–
Shortening	%	18%	14%	12%	17%
<i>Amount of subduction at 25% bulk shortening</i>					
Model slab length along section A	cm	0	3	3	–
Scaled slab length	km	0	75	75	210 km
Model slab length along section B	cm	0	2.4	0.6	–
Scaled slab length	km	0	60	15	0 km
Lateral decrease in slab length	%	–	20%	80%	100%

plate boundary continues to accommodate dextral displacements in response to upper plate extrusion. Within the upper plate the strike-slip faults strike at a high angle to the convergence direction, whereas the compressional structures strike (sub) perpendicular and terminate towards the weak lateral confinement. Similar to previous models an area developed where compressional, transpressive and strike-slip structures overlap. At 22% bulk shortening (Fig. 5a) the deformation on the subducting plate migrates towards the foreland near the confined margin but near the unconstrained margin the convergence is only accommodated by the initial pop-up. In the upper plate additional strike-slip faults occur with some minor new compressional structures. Overall, the amount of extrusion is limited with an elongation of 9% for the upper plate (Table 2).

The lithospheric mantle also displays a limited amount of extrusion, an elongation of 12%, which is significantly lower than in the previous experiments (Table 2). This is also reflected by the direction of the vectors, both at the bottom of the mantle layer and at the surface, where the vectors only have a small lateral component with respect to the convergence direction. The vector velocity is also very low in the upper plate, contrasting the high velocities of the lower plate for both the crust and the lithospheric mantle. Hence, the subduction and the associated crustal structures accommodate most of the shortening.

The cross-sections show a symmetric pop-up structure, situated above the subducting lithospheric mantle of the lower plate. In cross-section A (Fig. 5d) a second fore-thrust is present which is lacking in cross-section B, conform the surface observation and in line with significantly less lithospheric mantle subduction close to the weak confinement (cross-section B, Fig. 5d). The 80% decrease in the amount of subduction (Table 2) contrasts with experiment 2, with a decrease of only 20%. However, similar to experiment 2 is the decoupling of the lower plate at the level of the lower crust. Furthermore, the cross-sections indicate that the lower crust of the lower plate is affected by thickening, whereas the subducting mantle layer has maintained the same thickness with some minor distortions due to flexure. Lastly, the cross-sections display lim-

ited upper plate deformation, including no thickening of the lower crust or lithospheric mantle.

4. Key findings and discussion of the experimental results

4.1. Indentation versus subduction

Lateral extrusion coupled to lithosphere-scale indentation (experiment 1) yielded deformation geometries that are consistent with results obtained by Davy and Cobbold (1988) or Ratschbacher et al. (1991b) with the development of compressional structures near the confined margin and strike-slip faults near the weak lateral confinement. In between the deformational domains, an area of overlap can be observed where faults cross-cut and display transpressive strain. The strike-slip faults bound crustal blocks that are displaced towards the weak lateral confinement. Unlike previous analogue modelling studies (e.g., Faccenna et al., 1996; Ratschbacher et al., 1991b) experiment 1 did not reproduce extensional structures. The obtained lateral extrusion in experiment 1 occurred on the scale of the lithosphere, indicating that indentation can be governed by strength contrasts at the level of the mantle lithosphere (see the strength profiles in Fig. 2).

Lateral extrusion in the subduction settings also involved the extrusion of the entire lithosphere and produced similar patterns of deformation in the overriding plate compared to indentation models (Figs. 6a and 6d). This suggests that lateral extrusion is independent of the shortening mode (indentation vs subduction). Nevertheless, clear differences to the indentation models exist, including the presence of a compressional belt developing at the plate contact with propagating deformation towards the foreland. Due to significant strain localization at the subduction boundary less strain is transferred to the upper plate leading to less extrusion of the upper crust. Interestingly, the amount of extrusion accommodated by the lithospheric mantle in the upper plate appears to be independent of indentation or subduction under conditions that the system is advancing (Table 2).

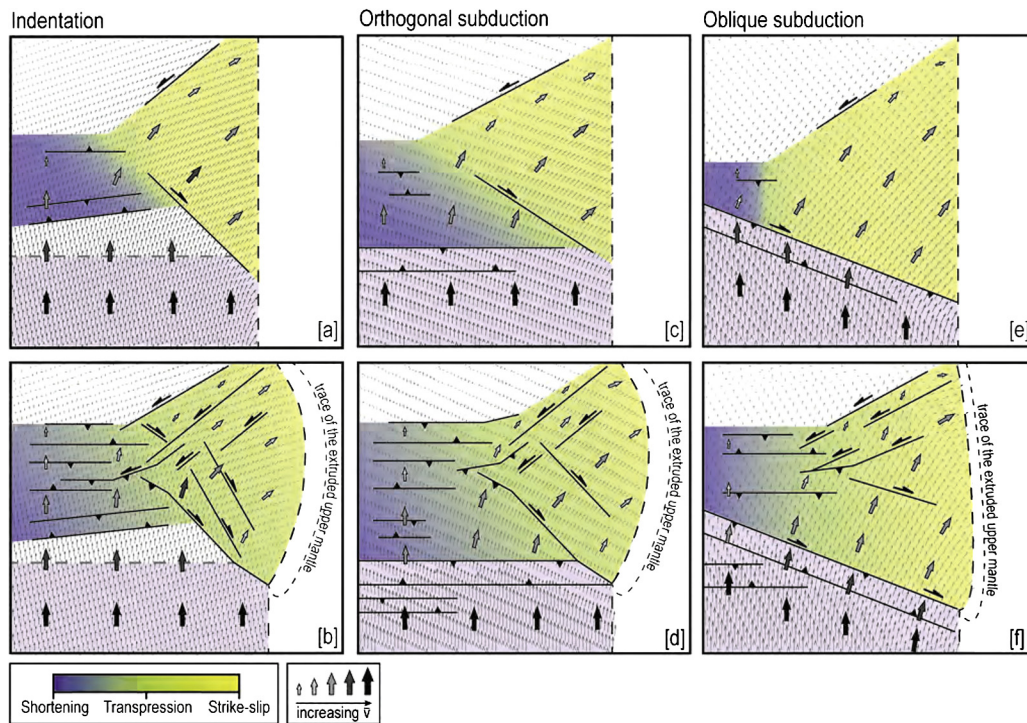


Fig. 6. Summary of the strain regimes and surface structures recorded through time and for the three separate scenarios: indentation [a–b], orthogonal subduction [c–d] and oblique subduction [e–f]. The two consecutive steps for each scenario show, according to the color coding, the transition from separate deformation domains to deformation characterized by a gradual transition of strain regimes. The stages are accompanied by indicative velocity fields and, for illustration purposes, representative vectors displaying the surface displacements, see legend. The grey shaded area defines the indenter or the lower plate.

The PIV analysis allows studying the distribution of strain in the upper plate through time at great detail. Separate kinematic domains were already described by [Rosenberg et al. \(2007\)](#), for instance, describing the transition from crustal thickening, near the confined margin, to transpression and strike-slip kinematics towards the weak or unconstrained margin. Based on a qualitative analysis of the obtained vector fields through time, in combination with the structural top-view analysis, a similar transition occurs in our models at 17% bulk shortening. However, prior to that only two separate kinematic domains are observed, namely compression and strike-slip (Figs. 6a and 6c). The lateral propagation of these domains subsequently resulted in the third, transpressional domain in between the initial two domains (Figs. 6b and 6d).

The PIV analysis also provides insights into the activation of faults. In all models the dextral strike-slip faults appear to accommodate a change in the direction of the surface displacements. During initial convergence the lateral component gradually increases, but with ongoing convergence the rotation is restricted to dextral faults creating a step-wise increase of the lateral component of displacement (Fig. 6). The sinistral and thrust faults are not associated with changes in displacement direction but are associated with changes in displacement velocity. Initially the displacement velocity decreased gradual with increasing distance to the plate boundary but during ongoing convergence the velocity decreases step-wise due to strain localization along the active sinistral and thrust faults.

4.2. Orthogonal versus oblique subduction

The most prominent difference between orthogonal and oblique subduction is the variable amount of subduction, which decreases rapidly in the case of oblique subduction by ca. 80% in the direction of the weak lateral confinement. In the case of a straight plate boundary the decrease is only 20% (Table 2). Furthermore, characteristic for the models with oblique subduction is that strain is par-

titioned into dip-slip and strike-slip displacements along the plate contact, where structures strike parallel to the plate boundary. The effect of strain partitioning is largest at the plate contact zone and diminishes with increasing distance to it, where the orientations of the structures largely develop perpendicular to the overall shortening direction. Similar behavior has been documented for oblique convergence along the Sumatran Fault system ([Martin et al., 2014; Morley, 2009](#)) or along the Andes ([Alvarado et al., 2016](#)). The natural scenarios demonstrate that strain partitioning can increase along the plate boundary, leading to slip reorganization, in response to a higher degree of obliquity. In our models an increase of dextral strike-slip displacements is notable towards the weak lateral confinement whilst the other end of the plate boundary is dominantly affected by dip-slip kinematics. In our case, this is not a response to a higher obliquity but related to the changing mode of deformation in the upper plate, i.e. from shortening to strike-slip.

The structures in the upper plate are significantly different to the experiments with orthogonal convergence (Fig. 6). For instance, the lack of dextral faults is an evident difference which could be the direct result of the strain partitioning along the collisional belt accommodating significant dextral displacement. As previously discussed, dextral faults are associated with rotations of the displacement vectors, which is conform to a large increase of the lateral component of displacement across the fold and thrust belt on top of the subduction boundary. As such, lateral extrusion is largest in close proximity to the lower plate as indicated by the direction of the displacement vectors that have the largest lateral component in close proximity to the plate contact (Fig. 6). This is significantly different to models with an orthogonal indentation or subduction boundary, where the highest degree of lateral extrusion occurs along the central axis of the upper plate, i.e. far away from the plate contact. We also note that the overall amount of lateral extrusion is less compared to models with a straight plate boundary (Table 2).

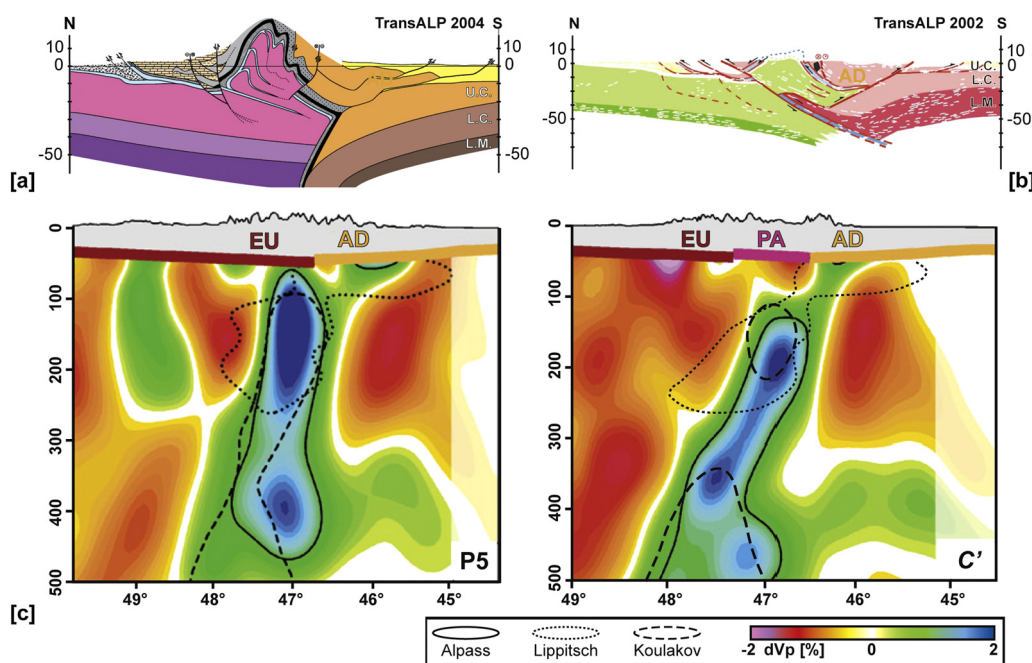


Fig. 7. [a] Interpretation of the structure of the Eastern Alps along the TransAlp transect (see the location of the TA-transect in Fig. 1b) according to Schmid et al. (2004) of the western part of the Eastern Alps traversing the Tauern Window and the Southern Alps. The Southern Alps sit on the Adriatic plate which features a 'crocodile style' subduction. The same transect is shown in [b] but interpreted by (TRANSALP Working Group, 2002) featuring a 'crocodile style' subduction of the European plate. [c] Two tomographic transects across the Eastern Alps by Mitterbauer et al. (2011) outlining the interpreted subducted material by the former and by Lippitsch et al. (2003) and Koulakov et al. (2009). The location of the two transects are presented in Fig. 1b. Abbreviations: upper crust (UC), lower crust (LC), lithospheric mantle (LM), European lithosphere (EU), Adriatic lithosphere (AD), Pannonian-Alpine lithosphere (PA).

5. Application to the Eastern Alps and other lateral extrusion scenarios

5.1. Lateral extrusion coeval with indentation or subduction?

Teleseismic tomography of the Eastern Alps (Fig. 1c and Fig. 7b) shows a high velocity anomaly, which has been interpreted as subducted Adriatic mantle lithosphere by Lippitsch et al. (2003). As a consequence, lateral extrusion in the Eastern Alps should have occurred on the upper plate, coeval with subduction rather than lithospheric-scale indentation of the Adriatic plate. In the light of this discussion, the experiments demonstrate that the first order deformation patterns, characteristic for lateral extrusion, are obtained in the case of lithosphere-scale indentation but also in the case of subduction. The insensitivity of extrusion to the mode of shortening confirms that an unconfined margin, as analogue for back-arc extension in the Pannonian basin, exerts the most important control on extrusion to occur (Ratschbacher et al., 1991b). Similar relationships are observed in other regions where, for example, roll-back in the Hellenic subduction system (Jolivet and Brun, 2010) or active extension in the southeast Asian orogenic system (Yin, 2010) provide an efficient mechanism for accommodating the escape of lithospheric blocks into their extensional domains. However, there are also distinct differences which we will use to compare the phenomenological characteristics and to shed new light on the discussion of indentation versus subduction in the Eastern Alps.

In the model with indentation no shortening was accommodated by the indenter, despite the similarity in upper crustal strength and only limited strength contrast in the lower crust (Fig. 2). However, early to late Miocene lateral extrusion in the Eastern Alps (e.g., Frisch et al., 2000; Wölfler et al., 2011) coincides with south directed propagation of a fold and thrust belt, i.e. the 'Southern Alps' (Fig. 1), on the Adriatic plate during late early Miocene to Pliocene times (Castellarin and Cantelli, 2000). It is unlikely that this fold and thrust belt, which is still active today (Benedetti et al., 2000), is the retro-wedge to the Eastern

Alps (Fig. 7b) at that time because it post-dates the main phase of northward propagation of the Eastern Alps (Beidinger and Decker, 2016; Rosenberg and Berger, 2009). Instead we follow in our interpretation Schmid et al. (2004) and propose that shortening in the Southern Alps is the crustal expression of subduction of the Adriatic mantle lithosphere (Fig. 7b), which is different to the Central Alps, where the Adriatic plate is not subducting and the Periadriatic Line acts as a major back-thrust transporting the European-onto the Adriatic crust (Schmid et al., 1996). The surface displacement velocities in our subduction models further support this idea; a strong decrease in velocity (1 cm/h to >0.6 cm/h, see Figs. 4 and 5) is observed when traversing the compressional belt along the plate boundary, whilst the model with indentation features a gradual decrease. This sudden decrease in displacement velocity is very similar to the observed decrease in GPS velocities when traversing the Periadriatic fault, i.e. passing from the Southern Alps to the Eastern Alps (Fig. 1b; Metois et al., 2015). On the contrary, GPS data for the Tibetan plateau and India does not show this significant drop in displacement velocity (Gan et al., 2007) suggesting the ongoing escape of the plateau is in response to indentation rather than subduction, conform a model with slab break-off events (Replumaz et al., 2014).

5.2. Orthogonal or oblique Adria-Alps convergence?

The interpretation of the orogen-scale structure of the Eastern Alps (Figs. 7a and b), based on reflection seismic profiling (TRANSALP Working Group, 2002) by Schmid et al. (2004) includes subduction of the Adriatic plate with a 'crocodile style' geometry split at the level of the upper crust. The cross-sections of experiments 2 and 3 show similar geometries (e.g. Fig. 5d), although in our case the lower plate is split at the level of the lower crust. Further to the east the Eastern Alps are affected by less crustal shortening and thus less thickening towards the Pannonian Basin (Rosenberg and Berger, 2009). Such lateral variance is observed in all models, but is especially obvious in the case of oblique convergence (experiment 3).

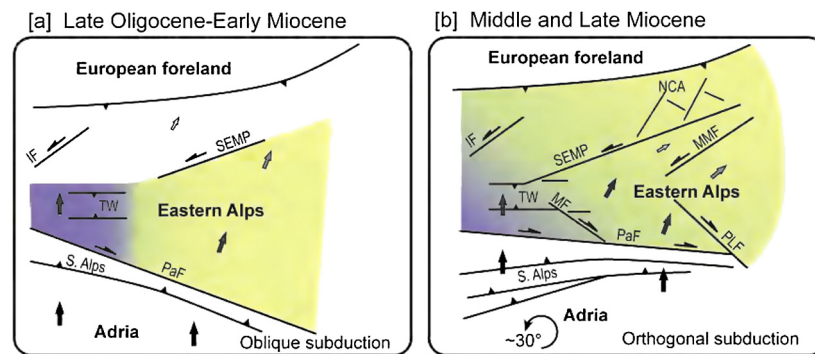


Fig. 8. A schematic two-stage tectonic evolution of the Eastern Alps, a) Late Oligocene–Early Miocene oblique convergence, and b) orthogonal convergence during the Middle and Late Miocene. See Fig. 6 for the used color coding. The black arrows are indicative displacement vectors for the two events (see Fig. 6). The figure is based on reconstructions presented by Wölfler et al. (2011) and Favaro et al. (2015). Abbreviations: Southern Alps (S. Alps), Periadriatic Fault (PaF), Tauern Window (TW), Inntal Fault (IF), Salzach–Ennstal–Mariazell–Puchberg (SEMP), Mur–Mürz Fault (MMF), Mölltal Fault (MF), Pöls–Lavanttal Fault (PLF), Northern Calcareous Alps (NCA).

Field studies suggest that oblique convergence was partitioned along networks of ductile and brittle transpressive structures in the surroundings of the Periadriatic fault system (Fig. 1b; Handy et al., 2005; Polinski and Eisbacher, 1992) leading to decreasing amounts of dextral offset in westerly direction (Linzer et al., 2002) and the formation of local transpressive fold and thrust belts (Polinski and Eisbacher, 1992). These observations are similar to the transpressive structures along the plate boundary in experiment 3 where dextral displacement increases towards the unconstrained margin from ca. 0.1 cm to more than 1 cm.

Even though our oblique experiment predicts significant dextral offset (cm scale) along the Periadriatic line and small offsets (mm scale) along sinistral faults at distance to the plate boundary, it fails to produce conjugate dextral and sinistral strike-slip faults like the Pöls–Lavanttal and the Mur–Mürz faults, respectively, in close proximity to the Pannonian Basin. Conversely, our experiments with orthogonal convergence fail to produce dextral offset along the plate boundary. In the Eastern Alps the transpressive Periadriatic fault was active between 35 Ma to at least 15 Ma (Handy et al., 2015, and references therein), and coexisted with the faults that have been active before the middle Miocene, like the sinistral Inntal and SEMP faults (Glodny et al., 2008; Wölfler et al., 2008, and references therein). However, from the middle Miocene onwards no significant dextral displacements are recorded along the Periadriatic fault but dextral displacement is concentrated along the dextral Pöls–Lavanttal and sinistral displacements are concentrated along the Mur–Mürz fault farther in the east (Fig. 1b; e.g., Reischenbacher and Sachsenhofer, 2013, and references therein). The former also displaced the Periadriatic fault and thus limits its main activity to pre-middle Miocene.

Based on our modelling results in combination with the above described field correlations we propose a transition from oblique to orthogonal convergence at the start of the middle Miocene (Fig. 8) providing valuable insights for the tectonic response in the Eastern Alps to the proposed change in Adriatic plate motion by Caputo et al. (2010) or a ca. 20° counterclockwise rotation of Adria and the Eastern Alps (Márton, 2000; Márton et al., 2003). A similar scenario was previously proposed by Neubauer et al. (1999), but lacks an explanation for the contemporaneous localization of shear along the Periadriatic fault and the SEMP fault. In our case, initial oblique convergence would be in line with the simultaneous activation of the SEMP and the Periadriatic fault with the latter being the effect of strain partitioning along the plate boundary.

5.3. Adriatic continental subduction with variable slab length

Tomographic imaging beneath the Eastern Alps (Fig. 1c) suggests that the Adriatic slab length decreases towards the east;

beneath the eastern Tauern Window the slab is ca. 210 km but beneath the Eastern Alps–Pannonian Basin transition it is not resolved by the tomography anymore. Our experiments show an 80% decrease of continental subduction towards the weak lateral confinement in oblique convergence and 20% in orthogonal convergence, respectively (Table 2 and Figs. 4 and 5). Such a significant reduction took place without any lateral change in the bulk amount of shortening but an increasing amount of the shortening is taken up by lateral transport of the upper plate towards the weak lateral confinement by an increase in the amount of dextral shear. Such a mechanism is in agreement with the observation that the amount of dextral strike-slip along the Periadriatic fault increases eastwards (e.g., Linzer et al., 2002), while the positive velocity anomaly beneath the Eastern Alps rapidly decreases in the same direction. Therefore, oblique subduction provides a viable explanation for the geometry of the positive mantle anomaly beneath the Eastern Alps, in which the material input in the subduction zone was gradually taken up by the eastward escape of the upper plate towards the Pannonian Basin.

5.4. Lateral extrusion: a lithospheric scale process

Lateral extrusion in the Eastern Alps has been interpreted as a crustal scale process (Horváth et al., 2006; Ziegler and Dèzes, 2006). However, a crustal scale extrusion contradicts a proposed upper mantle flow described by Kummerow and Kind (2006), and Qorbani et al. (2015) documenting mantle anisotropy which is parallel to surface deformation. This could imply that the upper mantle is also involved in extrusion, an aspect that has not been analyzed in previous analogue models.

Our experiments, which assume that the intended crust is underlain by a weak mantle lithosphere, show extrusion of the entire lithosphere rather than solely the crust (Figs. 3 to 5). We observe systematically more lithospheric mantle extrusion suggesting that the mantle is at least partly decoupled from the overlying crust, supporting views that the mantle could be of great influence in driving extrusion at crustal levels. As such, the flow of the mantle lithosphere might be more important than hitherto assumed, which is in line with numerical modelling results that visualize sub-lithospheric flow during extrusion of the Tibetan plateau or the Anatolian plateau into the Aegean (e.g., Sternai et al., 2014). Hence, we suggest that the strong control of deep seated processes on surface deformation would reduce the call for strong strength contrasts between the indenter and the indented region.

6. Conclusions

A series of analogue models have been performed to study the tectonic response of subduction on lateral extrusion of the upper

plate. The experiments illustrate that lateral extrusion can occur above a subducting plate and that the deformation and strain propagation in the upper plate is similar to classical indentation models. In both cases the upper plate displays a transition from compressional structures near the confined boundary, to strike-slip structures towards the weak lateral boundary. During initial convergence we observe a rapid transition of strain but with ongoing convergence the transition becomes gradual with an area of transpressive structures amid. The surface deformation has a strong similarity with lateral extrusion structures in the Eastern Alps even though no extensional structures were obtained. Both indentation and subduction are valid mechanisms to explain the deformation patterns in the Eastern Alps, but only subduction of the Adriatic plate leads to the foreland propagating thrusts as observed in the Southern Alps.

When incorporating oblique convergence the upper plate deformation is minimal and accommodates little extrusion. A striking difference with orthogonal convergence is the presence of strain partitioning along the plate boundary. This observed tectonic response bears significant similarities with the kinematics of the Peri-Adriatic fault, marking the transition from the Adriatic plate to the Eastern Alps. As a consequence of strain partitioning and increasing dextral slip along the plate boundary the amount of subduction decreases towards the weak lateral confinement. This has a striking resemblance to the rapid decrease in the Adriatic slab length beneath the Eastern Alps and implies continental subduction of Adria that is not genetically linked to other slabs in the vicinity.

Based on the experimental results we propose that the Eastern Alps are characterized by an initial phase of oblique convergence but are consequently affected by orthogonal convergence from middle Miocene onwards. We attribute this change to the frequently documented Miocene switch in plate motion of Adria.

Acknowledgement

This research has been funded by the Netherlands research centre for Integrated Solid Earth Sciences (ISES). We would like to thank the reviewers (Anne Replumaz, Marco Bonini and Lothar Ratschbacher) for their detailed feedback which greatly improved the manuscript. We thank Elisa Calignano for sharing her practical and theoretical knowledge of analogue models and Joost van der Broek for technical support in the TecLab. Support and detailed instructions by Karen Leever for the PIV analysis was greatly appreciated. Additional modeling results and data supporting this research is available by contacting the corresponding author or sending an email to the Tectonics group at the Utrecht University (uu.teclab@gmail.com).

Appendix A. Supplementary material

Supplementary material related to this article can be found online at <http://dx.doi.org/10.1016/j.epsl.2017.05.012>.

References

- Alvarado, A., Audin, L., Nocquet, J.M., Jaillard, E., Mothes, P., Jarrín, P., Segovia, M., Rolandone, F., Cisneros, D., 2016. Partitioning of oblique convergence in the Northern Andes subduction zone: migration history and the present-day boundary of the North Andean Sliver in Ecuador. *Tectonics* 35, 1048–1065.
- Beidinger, A., Decker, K., 2016. Paleogene and Neogene kinematics of the Alpine–Carpathian fold-thrust belt at the Alpine–Carpathian transition. *Tectonophysics* 690, 263–287.
- Benedetti, L., Tapponnier, P., King, G.C.P., Meyer, B., Manighetti, I., 2000. Growth folding and active thrusting in the Montello region, Veneto, northern Italy. *J. Geophys. Res., Solid Earth* 105, 739–766.
- Caputo, R., Poli, M.E., Zanferrari, A., 2010. Neogene–Quaternary tectonic stratigraphy of the eastern Southern Alps, NE Italy. *J. Struct. Geol.* 32, 1009–1027.
- Castellarin, A., Cantelli, L., 2000. Neo-Alpine evolution of the Southern Eastern Alps. *J. Geodyn.* 30, 251–274.
- Davy, P., Cobbold, P.R., 1988. Indentation tectonics in nature and experiment, 1: experiments scaled for gravity. *Bull. Geol. Inst. Univ. Upps.* 14, 129–141.
- Davy, P., Cobbold, P.R., 1991. Experiments on shortening of a 4-layer model of the continental lithosphere. *Tectonophysics* 188, 1–25.
- Faccenna, C., Davy, P., Brun, J.P., Funicello, R., Giardini, D., Mattei, M., Nalpas, T., 1996. The dynamics of back-arc extension: an experimental approach to the opening of the Tyrrhenian Sea. *Geophys. J. Int.* 126, 781–795.
- Favaro, S., Schuster, R., Handy, M.R., Scharf, A., Pestal, G., 2015. Transition from orogen-perpendicular to orogen-parallel exhumation and cooling during crustal indentation – key constraints from Sm-147/Nd-144 and Rb-87/Sr-87 geochronology (Tauern Window, Alps). *Tectonophysics* 665, 1–16.
- Frisch, W., 1998. Palinspastic reconstruction and topographic evolution of the Eastern Alps during late Tertiary tectonic extrusion. *Tectonophysics* 297, 1–15.
- Frisch, W., Dunkl, I., Kulemann, J., 2000. Post-collisional orogen-parallel large-scale extension in the Eastern Alps. *Tectonophysics* 327, 239–265.
- Gan, W., Zhang, P., Shen, Z.-K., Niu, Z., Wang, M., Wan, Y., Zhou, D., Cheng, J., 2007. Present-day crustal motion within the Tibetan Plateau inferred from GPS measurements. *J. Geophys. Res., Solid Earth* 112, 1–14.
- Glodny, J., Ring, U., Kuhn, A., 2008. Coeval high-pressure metamorphism, thrusting, strike-slip, and extensional shearing in the Tauern Window, Eastern Alps. *Tectonics* 27 (4), TC4004.
- Handy, M.R., Babist, J., Wagner, R., Rosenberg, C., Konrad, M., 2005. Decoupling and its relation to strain partitioning in continental lithosphere: insight from the Peri-Adriatic fault system (European Alps). *Geol. Soc. (Lond.) Spec. Publ.* 243, 249–276.
- Handy, M.R., Ustaszewski, K., Kissling, E., 2015. Reconstructing the Alps–Carpathians–Dinarides as a key to understanding switches in subduction polarity, slab gaps and surface motion. *Int. J. Earth Sci.* 104, 1–26.
- Horváth, F., Bada, G., Szafian, P., Tari, G., Adam, A., Cloetingh, S., 2006. Formation and deformation of the Pannonian Basin: constraints from observational data. *Mem. Geol. Soc. Lond.* 32, 191–206.
- Iaffaldano, G., Di Giuseppe, E., Corbi, F., Funicello, F., Faccenna, C., Bunge, H.P., 2012. Varying mechanical coupling along the Andean margin: implications for trench curvature, shortening and topography. *Tectonophysics* 526–529, 16–23.
- Jolivet, L., Brun, J.P., 2010. Cenozoic geodynamic evolution of the Aegean. *Int. J. Earth Sci.* 99, 109–138.
- Koulakov, I., Kaban, M.K., Tesauro, M., Cloetingh, S., 2009. P- and S-velocity anomalies in the upper mantle beneath Europe from tomographic inversion of ISC data. *Geophys. J. Int.* 179, 345–366.
- Kummerow, J., Kind, R., 2006. Shear wave splitting in the Eastern Alps observed at the TRANSALP network. *Tectonophysics* 414, 117–125.
- Leever, K.A., Gabrielsen, R.H., Sokoutis, D., Willingshofer, E., 2011. The effect of convergence angle on the kinematic evolution of strain partitioning in transpressional brittle wedges: insight from analog modeling and high-resolution digital image analysis. *Tectonics* 30.
- Linzer, H.-G., Decker, K., Peresson, H., Dell'Mour, R., Frisch, W., 2002. Balancing lateral orogenic flow of the Eastern Alps. *Tectonophysics* 354, 211–237.
- Lippitsch, R., Kissling, E., Ansorge, J., 2003. Upper mantle structure beneath the Alpine orogen from high-resolution teleseismic tomography. *J. Geophys. Res., Solid Earth* 108, ESE 5–1–ESE 5–15.
- Luth, S., Willingshofer, E., Sokoutis, D., Cloetingh, S., 2010. Analogue modelling of continental collision: influence of plate coupling on mantle lithosphere subduction, crustal deformation and surface topography. *Tectonophysics* 484, 87–102.
- Martin, K.M., Gulick, S.P.S., Austin Jr, J.A., Berglar, K., Franke, D., Udrek, 2014. The west Andaman fault: a complex strain-partitioning boundary at the seaward edge of the Aceh basin, offshore Sumatra. *Tectonics* 33, 786–806.
- Márton, E., 2000. Miocene rotations in the Eastern Alps: palaeomagnetic results from intramontane basin sediments. *Tectonophysics* 323, 163–182.
- Márton, E., Drobne, K., Čosović, V., Moro, A., 2003. Palaeomagnetic evidence for Tertiary counterclockwise rotation of Adria. *Tectonophysics* 377, 143–156.
- McKenzie, D.P., 1972. Active tectonics of the Mediterranean region. *Geophys. J. R. Astron. Soc.* 30, 109–185.
- Metois, M., D'Agostino, N., Avallone, A., Chamot-Rooke, N., Rabaut, A., Duni, L., Kuka, N., Koci, R., Georgiev, I., 2015. Insights on continental collisional processes from GPS data: dynamics of the peri-Adriatic belts. *J. Geophys. Res., Solid Earth* 120, 8701–8719.
- Mitterbauer, U., Behm, M., Bruckl, E., Lippitsch, R., Guterch, A., Keller, G.R., Koslovskaya, E., Rumpfhuber, E.M., Sumanov, F., 2011. Shape and origin of the East-Alpine slab constrained by the ALPASS teleseismic model. *Tectonophysics* 510, 195–206.
- Morley, C.K., 2009. Evolution from an oblique subduction back-arc mobile belt to a highly oblique collisional margin: the Cenozoic tectonic development of Thailand and eastern Myanmar. *Geol. Soc. (Lond.) Spec. Publ.* 318, 373–403.
- Neubauer, F., Genser, J., Kurz, W., Wang, X., 1999. Exhumation of the Tauern window, Eastern Alps. *Phys. Chem. Earth, Part A, Solid Earth Geod.* 24, 675–680.
- Polinski, R.K., Eisbacher, G.H., 1992. Deformation partitioning during polyphase oblique convergence in the Karawanken Mountains, southeastern Alps. *J. Struct. Geol.* 14, 1203–1213.

- Qorbani, E., Kurz, W., Bianchi, I., Bokermann, G., 2015. Correlated crustal and mantle deformation in the Tauern Window, Eastern Alps. *Austrian J. Earth Sci.* 108, 159–171.
- Ramberg, H., 1981. *Gravity, Deformation and the Earth's Crust*, 2nd edition. Academic Press, London.
- Ratschbacher, L., Frisch, W., Linzer, H.G., Merle, O., 1991a. Lateral extrusion in the Eastern Alps, part 2: structural analysis. *Tectonics* 10, 257–271.
- Ratschbacher, L., Merle, O., Davy, P., Cobbald, P., 1991b. Lateral extrusion in the eastern Alps, part 1: boundary conditions and experiments scaled for gravity. *Tectonics* 10, 245–256.
- Reischenbacher, D., Sachsenhofer, R.F., 2013. Basin formation during the post-collisional evolution of the Eastern Alps: the example of the Lavanttal Basin. *Int. J. Earth Sci.* 102, 517–543.
- Replumaz, A., Capitanio, F.A., Guillot, S., Negredo, A.M., Villasenor, A., 2014. The coupling of Indian subduction and Asian continental tectonics. *Gondwana Res.* 26, 608–626.
- Robl, J., Stüwe, K., 2005. Continental collision with finite indenter strength, 2: European Eastern Alps. *Tectonics* 24.
- Rosenberg, C.L., Berger, A., 2009. On the causes and modes of exhumation and lateral growth of the Alps. *Tectonics* 28, 1–19.
- Rosenberg, C.L., Brun, J.P., Cagnard, F., Gapais, D., 2007. Oblique indentation in the Eastern Alps: insights from laboratory experiments. *Tectonics* 26, 1–23.
- Schmid, S.M., Fügenschuh, B., Kissling, E., Schuster, R., 2004. Tectonic map and overall architecture of the Alpine orogen. *Eclogae Geol. Helv.* 97, 92–117.
- Schmid, S.M., Pfiffner, O.A., Froitzheim, N., Schönborn, G., Kissling, E., 1996. Geophysical-geological transect and tectonic evolution of the Swiss–Italian Alps. *Tectonics* 15, 1036–1064.
- Sokoutis, D., Bonini, M., Medvedev, S., Boccaletti, M., Talbot, C.J., Koyi, H., 2000. Indentation of a continent with a built-in thickness change: experiment and nature. *Tectonophysics* 320, 243–270.
- Sokoutis, D., Burg, J.P., Bonini, M., Corti, G., Cloetingh, S., 2005. Lithospheric-scale structures from the perspective of analogue continental collision. *Tectonophysics* 406, 1–15.
- Sokoutis, D., Willingshofer, E., 2011. Decoupling during continental collision and intra-plate deformation. *Earth Planet. Sci. Lett.* 305, 435–444.
- Sternai, P., Jolivet, L., Menant, A., Gerya, T., 2014. Driving the upper plate surface deformation by slab rollback and mantle flow. *Earth Planet. Sci. Lett.* 405, 110–118.
- Sveen, J., 2004. An introduction to MatPIV v. 1.6.1. *Mechanics and Applied Mathematics*, University of Oslo, Oslo.
- Tapponnier, P., Peltzer, G., Armijo, R., 1986. *On the mechanics of the collision between India and Asia*. Geological Society, London.
- TRANSALP Working Group, 2002. First deep seismic reflection images of the eastern Alps reveal giant crustal wedges and transcrustal ramps. *Geophys. Res. Lett.* 29, 1452.
- Ustaszewski, K., Schmid, S.M., Fügenschuh, B., Tischler, M., Kissling, E., Spakman, W., 2008. A map-view restoration of the Alpine–Carpathian–Dinaridic system for the Early Miocene. *Swiss J. Geosci.* 101, 273–294.
- Weijermars, R., Schmeling, H., 1986. Scaling of Newtonian and non-Newtonian fluid dynamics without inertia for quantitative modelling of rock flow due to gravity (including the concept of rheological similarity). *Phys. Earth Planet. Inter.* 43, 316–330.
- Westerweel, J., 1997. Fundamentals of digital particle image velocimetry. *Meas. Sci. Technol.* 8, 1379–1392.
- Willingshofer, E., Cloetingh, S., 2003. Present-day lithospheric strength of the Eastern Alps and its relationship to neotectonics. *Tectonics* 22, 1075–1075.
- Willingshofer, E., Sokoutis, D., Burg, J.P., 2005. Lithospheric-scale analogue modelling of collision zones with a pre-existing weak zone. In: Gapais, D., Brun, J.P., Cobbald, P.R. (Eds.), *Deformation Mechanisms, Rheology and Tectonics: From Minerals to the Lithosphere*, pp. 277–294.
- Wölfler, A., Dekant, C., Danišik, M., Kurz, W., Dunkl, I., Putiš, M., Frisch, W., 2008. Late stage differential exhumation of crustal blocks in the central Eastern Alps: evidence from fission track and (U–Th)/He thermochronology. *Terra Nova* 20, 378–384.
- Wölfler, A., Kurz, W., Fritz, H., Stüwe, K., 2011. Lateral extrusion in the Eastern Alps revisited: refining the model by thermochronological, sedimentary, and seismic data. *Tectonics* 30, 1–15.
- Yin, A., 2010. Cenozoic tectonic evolution of Asia: a preliminary synthesis. *Tectonophysics* 488, 293–325.
- Ziegler, P.A., Dèzes, P., 2006. *Crustal evolution of Western and Central Europe*, vol. 32. Geological Society, London, Memoirs, pp. 43–56.